Nanoscale Advances

Accepted Manuscript

This article can be cited before page numbers have been issued, to do this please use: Q. Han, H. Wang, Y. Qi, D. Wu and Q. Wei, *Nanoscale Adv.*, 2019, DOI: 10.1039/C9NA00394K.

ROYAL SOCIETY OF CHEMISTRY

rsc.li/nanoscale-advances

View Article Online
DOI: 10.1039/C9NA00394K

Preparation, characterization of 0D Au NPs@3D BiOI nanoflowers/2D NiO nanosheet arrays heterostructure and application for a self-powered photoelectrochemical biosensing platform

Qingzhi Han, Hanyu Wang, Yanting Qi, Dan Wu*, Qin Wei

Key Laboratory of Interfacial Reaction & Sensing Analysis in Universities of Shandong, University of Jinan, Jinan 250022, PR China

* Corresponding author

Email address: wudan791108@163.com; Tel: + 86-531-82767872

View Article Online
DOI: 10.1039/C9NA00394K

Abstract

In this work, we demonstrate that the zero-dimensional Au nanoparticles (0D Au NPs) decorated three-dimensional bismuth oxyiodide (BiOI) nanoflowers (3D BiOI NFs)/two-dimensional nickel oxide (NiO) nanosheet arrays (2D NiO NSAs) hybrid nanostructure can be used as a self-powered cathodic photoelectrochemical (PEC) biosensing platform. The in situ formation of 3D BiOI NFs onto 2D NiO NSAs was by a chemical bath deposition method, while 0D Au NPs coated on 3D BiOI NFs/2D NiO NSAs was through a dip-coating method. Subsequently, glucose oxidase (GOD) as enzyme model was immobilized on the surface of Au@BiOI/NiO electrode via the adhesion effect of poly-(diallyldimethylammonium chloride) (PDDA). The proposed heterostructure exhibited excellent PEC properties is because the unique structure of Au NPs@BiOI NFs/NiO NSAs increased its specific surface area and light harvest ability, as well as the assistance of surface plasmon resonance effect of Au NPs. The system displayed high sensitivity toward glucose with the presence of air saturated electrolyte. At the optimum conditions, the biosensor showed a promising application for self-powered cathodic PEC biosensing of glucose, with a dynamic linear range of 1×10^{-7} M ~ 5×10^{-2} M and a low limit of detection of 8.71×10^{-8} M. Moreover, the proposed self-powered PEC biosensor was evaluated for the determination of diluted glucose injections, the results indicating the potential of the proposed biosensor for the bioanalysis applications.

Keywords: self-powered; Au@BiOI/NiO; surface plasmon resonance; photoelectrochemical; biosensor; photocathode

View Article Online
DOI: 10.1039/C9NA00394K

Introduction

Since the first self-powered biosensor was reported by Katz E and Willner in 2001,[1] the self-powered biosensor gets more and more attention. In a typical self-powered sensing platform, it is the sensor itself who provide the power for the sensing device and don't need external power supply.[2-7] In other words, a self-powered photoelectrochemical (PEC) biosensor is an integrated device, which have both electronic power supply and biosensing functions.[8] These characteristics would benefit the fabrication process, economic efficiency, portability and miniaturization of the biosensors, which makes self-powered biosensor become a powerful and promising candidate in the immunoassay field, especially no-battery portable devices.[9-11] At present, with the development of nanomaterial science and nanotechnology, the structure design and application of semiconductors gets more and more attention. To obtain the desired PEC performance, the type, band gap size as well as the band matching of semiconductors all need judicious design and optimize.[12-15] Various heterostructures has been designed to expand the light utilization range or improve the electron (e^-)/hole (h^+) separation efficiency,[16] such as: Au NPs@ZnO,[17] CdS/RGO/ZnO,[3] CdSe/ZnS/TiO_2,[18] NiO/PbS[12] and C_3N_4/PbS.[19] The self-powered PEC biosensor could be divided in three major categories: p type/p-p heterostructure,[12] n type/n-n heterostructure[3, 4, 17] and photofuel cell type.[20]

For p-type semiconductor, it is the opposite of n-type semiconductor, which is more easily to react with electron acceptors (such as: dissolved oxygen) rather than electron donors (such as: glutathione, ascorbic acid, sodium sulfite) in the electrolyte, indicating their good potential in anti-interference from reducing substances.[12, 21, 22] In other words, the p-type semiconductor is more stable than n-type semiconductor in oxidation reactions.[23] As a popular p-type semiconductor, NiO (nickel oxide) has been widely used in the field of sensors, catalyzers and solar cells due to its good stability, unique electrochemical performance and excellent catalytic properties.[20, 24] BiOI (bismuth oxyiodide) as an ideal p-type photosensitize with narrow band gap (~ 1.7 eV), and possess wide visible light absorption range. When NiO and BiOI

combined together, the photochemical property would be improved greatly.[15] Based on NiO/BiOI heterostructure, we further added Au NPs on its surface, resulting in unique structure and significant improved photoelectrochemical activities.

In this work, we developed a novel self-powered PEC biosensor based on Au@BiOI/NiO heterostructure. In detail, we decorated the three-dimensional BiOI nanoflowers (3D BiOI NFs) onto the surface of two-dimensional NiO nanosheet arrays (2D NiO NSAs) via the chemical bath deposition (CBD) technique.[25] The narrow band-gap p-type semiconductor BiOI (E_g = 1.7 eV)[22, 25] enlarged the light absorption range of NiO (E_g = 3.5 eV)[22] and accelerated the e^-/h^+ separation rate of the BiOI/NiO heterostructure. Following, the zero-dimensional Au nanoparticles (0D Au NPs) was introduced by dip-coating method,[26] and formed Au@BiOI/NiO hybrid heterostructure. After the glucose-oxidase (GOD) was fixed on the Au@BiOI/NiO/ITO electrodes, the self-powered PEC biosensor for glucose detection was successfully constructed, as shown in scheme 1 below. Different from the previous reports,[15] the proposed sensor exhibits the traditional O_2-dependent signal suppression mechanism and exhibited a high sensitivity. Owing to the unique 0D Au@3D BiOI/2D NiO hybrid nanostructure as well as the good conductivity and SPR effect of Au NPs, compared with the similar work, [15] [12] the fabricated PEC biosensor showed better performance (lower LOD and wider detection range). Hence, the different material combination and structure design are very important aspects for the improvement performance of the PEC biosensor.

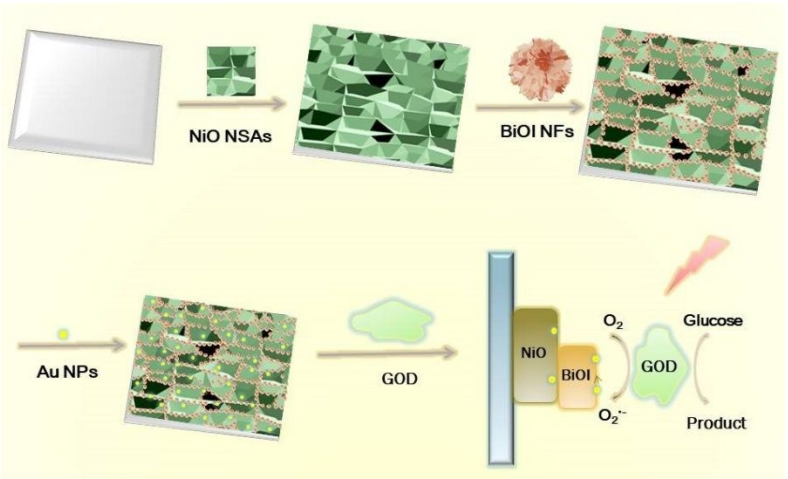

Scheme 1. Preparation of 0D Au NPs modified 3D BiOI NFs/2D NiO NSAs heterosctructure and

View Article Online
DOI: 10.1039/C9NA00394K

its application for glucose detection.

Experimental section

Chemicals and apparatus; synthesis of NiO, BiOI/NiO, and Au@BiOI/NiO; SEM of excess BiOI CBD repeating cycles; simulation parameters of the equivalent circuit components; comparison of various methods for the determination glucose; determination of glucose in diluted glucose injections have been supplied in Supporting Information.

Results and discussion

Characterization of the As-Prepared Materials. After $Ni(OH)_2$ (morphologies are shown in Figure S1) annealed at 400 ℃ for 2 h (under argon atmosphere), the obtained NiO (Figure 1A and 1B (SEM); Figure S2 A (TEM)) still kept the NSAs structure. Figure 1C illustrated that the XRD pattern of NiO was consistent with NiO (JCPDS PDF#44-1159-NiO), indicating the formation of NiO. Cross-sectional view demonstrated that the thickness of NiO on ITO is about 2.4 μm (Figure 1D). As depicted in the SEM (Figure 1E and 1F) and TEM of BiOI/NiO (Figure S2 B), the flower-like BiOI uniform arrangement in the surface of NiO NSAs, which would enlarge the specific surface area of NiO and provide more enzyme loading site. What's more, the highly ordered heterostructure also benefited the electron transfer in the BiOI/NiO and further enhanced the photocurrent. [3]

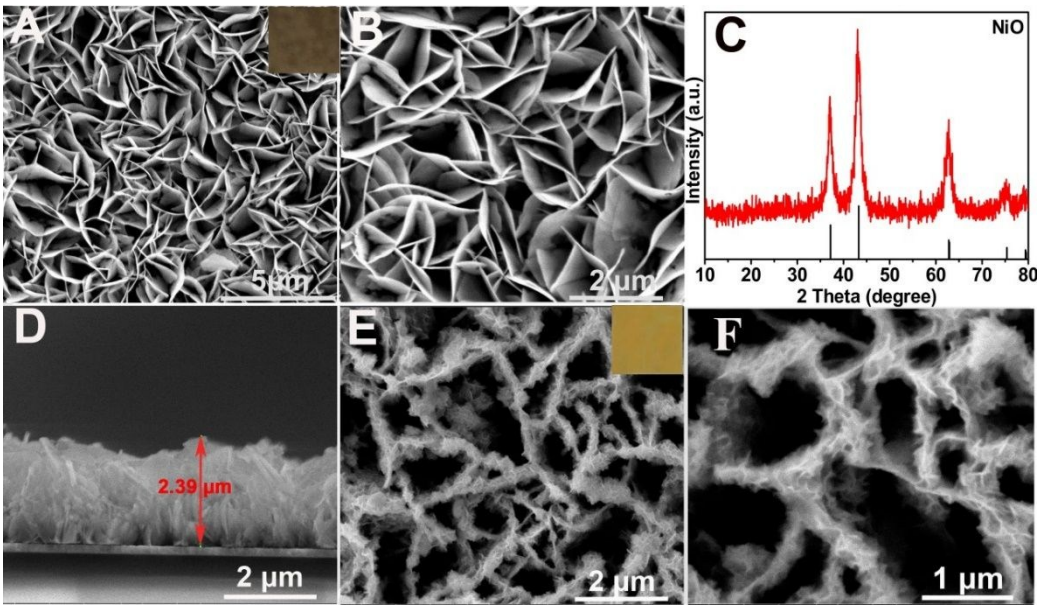

View Article Online
DOI: 10.1039/C9NA00394K

Figure 1. (A) SEM image of NiO NSAs. Inset is NiO coated ITO. (B) High-magnification SEM image of NiO NSAs. (C) XRD pattern of the as-fabricated NiO NSAs. (D) The cross-sectional view of NiO/ITO electrode. (E) SEM image of NiO/BiOI nanostructure. Inset shows its color. (F) High-magnification SEM image of NiO/BiOI.

The high-resolution transmission electron microscopic (HRTEM) of Au NPs was shown in Figure 2A, which has a diameter in the range of 12 ~ 14 nm (inset). Figure 2B depicted the SEM image of Au@BiOI/NiO hybrid nanostructure, as shown in the high magnification inset, the Au NPs are sparsely distributed on the surface of BiOI/NiO. The hybrid nanocomposites of the 0D Au NPs@BiOI/NiO is expected to have high electron-hole separation efficiency as well as surface plasmon resonance (SPR) effect[27]. As shown in Figure 2C, the EDS analysis revealed that O, Bi, I, Au, and Ni elements existed in the sample, indicating the Au@BiOI/NiO was synthesized successfully.

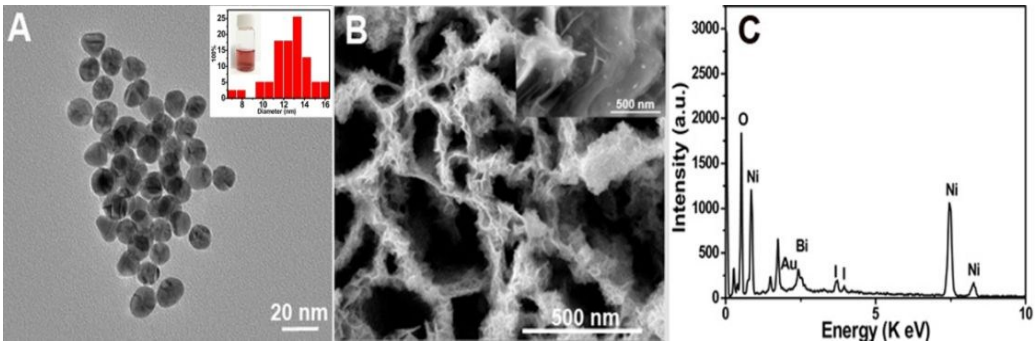

Figure 2. (A) HRTEM of the as-synthesized Au NPs; Inset: Au NPs size distribution and PVP-stabilized Au solution. (B) SEM image of Au NPs@BiOI NFs/NiO NSAs; Inset shows the magnified view. (C) The corresponding EDS spectrum of the Au NPs@BiOI NFs/NiO NSAs electrode.

Figure 3A, B, C, D, E and F offers the X-ray photoelectron spectroscopy (XPS) spectra of Au@BiOI/NiO survey, O1s,Ni 2p, Bi 4f, I 3d and Au 4f regions. Obviously, the elements of Ni, I, O, Bi, and Au were detected in the XPS survey spectrum (Figure 3A) in the range of 0 - 900 eV. C element in the spectrum (C 1s, 284.6 eV) was added as the internal standards. The asymmetric peak of the O 1s spectrum (Figure 3B) illustrated that there was more than one chemical state of O. The peaks at 531.4 and 529.1 eV can be assign to Ni-O, Bi-O, as well as the surface adsorption oxygen, respectively. Figure 3C depicted the XPS spectrum of Ni 2p, there are several peaks in the range of 851 - 882 eV. The peaks located at 853.1, 855.1, and

861.3 eV belonged to Ni-O bonding. Notably, the peaks located at 853.5, 860.4 eV and 872.4, 878.7 eV can be attribute to Ni $2p_{3/2}$ and Ni $2p_{1/2}$ as well as its satellite peaks, respectively. As Figure 3D suggested, the Bi 4f spectrum can be fitted to two distrinct peaks. The peaks centered at 158.6 and 164.0 eV are assigned to Bi $4f_{7/2}$ and Bi $4f_{5/2}$, respectively, which can be ascribed to Bi^{3+} in BiOI. Figure 3E showed the XPS spectrum of I 3d with two different peaks in the binding energy range of 615 - 635 eV. Particularly, the peaks located at ~631 and ~619 eV were assigned to I $3d_{3/2}$ and I $3d_{5/2}$, respectively. Two dissymmetrical binding energies peaks centered at 83.2 and 86.9 eV (Figure 3F) assigned to the the binding energies of Au $4f_{7/2}$ and Au $4f_{5/2}$, respectively. In addition, the deviations of the binding energies between these two peaks is 3.7 eV, according to the previous literature the Au NPs were existed in the metallic state.[28] Overall, the XPS spectrum proved the successful synthesis of Au@BiOI/NiO heterostructure.

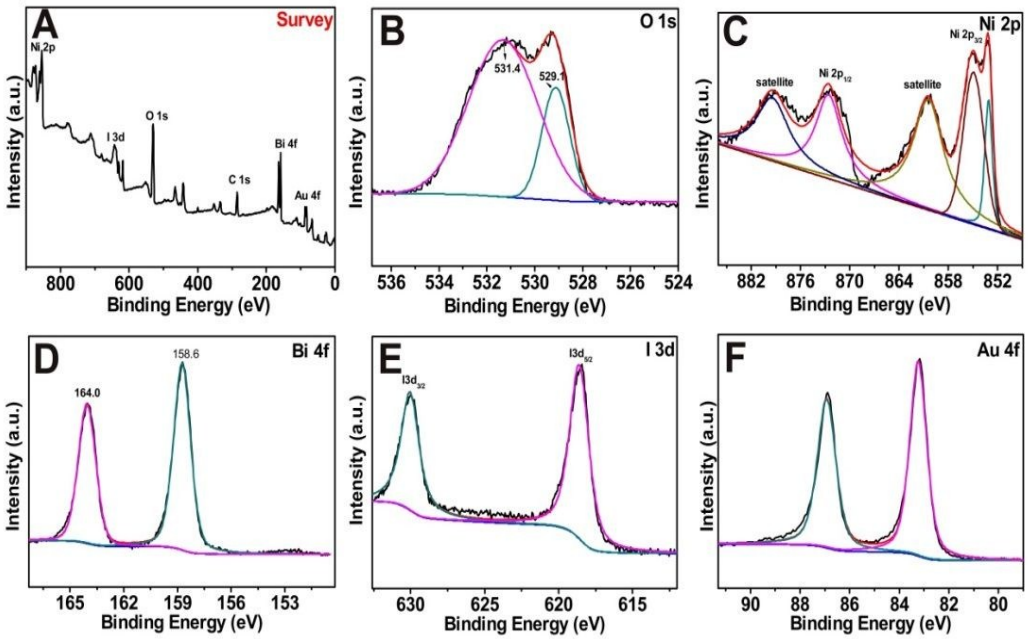

Figure 3. (A) XPS survey of the as-fabricated Au@/BiOI/NiO heterostructure and (B-F) high-resolution XPS spectra of O 1s, Ni 2p, Bi 4f, I 3d and Au 4f, respectively.

In proof of the formation of Au@NiO/BiOI, the as-prepared hybrid nanostructures were also characterized with Raman spectrum (Figure 4A) and UV-vis

absorption spectroscopy (Figure 4B). For Raman spectrum of NiO/BiOI (curve a), the peaks at 85 cm^{-1} and 154 cm^{-1} are assigned to the Bi-I vibration of BiOI.[29] The peaks located at 460 cm^{-1} could be attribute to the first-order transverse optical (TO) and longitudinal optical (LO) phonon modes of NiO, respectively.[30] The peaks located at ~ 1080 cm^{-1} ascribe to the 2 LO of NiO.[31] Compared with curve a, after the adding of Au NPs (curve b) the Raman intensity was enhanced slightly and the peaks have a certain displacement, which could be attributed to the formation of Au@BiOI/NiO as well as the plasmonic effect of Au NPs. As depicted in Figure 4B, the black curve is the UV-vis diffuse reflectance spectra of pure NiO, after the addition of BiOI the absorbance intensity was enhanced in the range of 300 ~ 580 nm. With the further addition of Au NPs (Figure 4B, blue curve), the absorption range was further enlarged. A small peaks located at ~ 525 nm could be attributed to the plasmonic effect of Au NPs.[27]

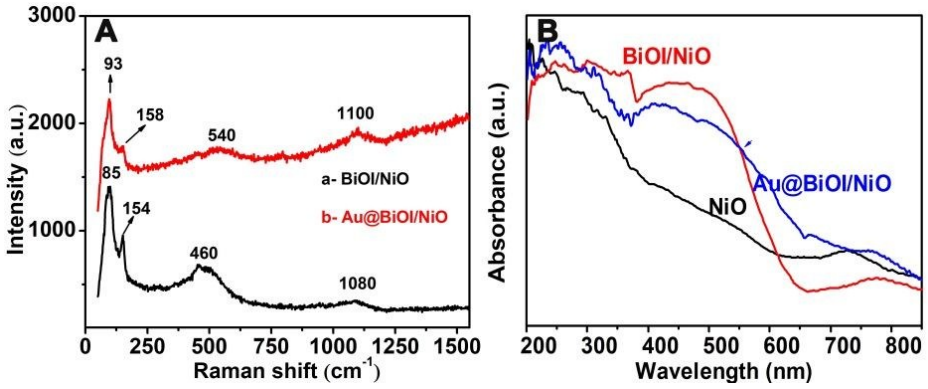

Figure 4. (A) Raman spectra (λ_{ex} = 532 nm) of the as-prepared NiO/BiOI/ITO and Au@NiO/BiOI/ITO samples. (B) UV-visible diffuse reflectance spectra of pure NiO, BiOI/NiO heterostructure and Au@BiOI/NiO hybrid nanocomposite.

Mechanism discussion of the constructed PEC biosensor

As presented in Scheme 2, the possible mechanism of the proposed PEC biosensor could be explained as follows: Under light irradiation, the photon-generated electron of BiOI/NiO could be transferred to the O_2 in Tris-HCl and form $O_2^{\cdot-}$. Because the SPR effect of Au NPs, Au also provide electron to the conduction band (CB) of BiOI and NiO, which would further enhance the photocurrent performance of BiOI/NiO. Besides, the good conductivity of Au also accelerates the electron transfer rate. At the same time, the GOD consumes O_2 to decompose glucose forming H_2O_2

and gluconic acid. Owing to the O_2 consumption competition between the GOD and Au@BiOI/NiO, the cathodic photocurrent intensity of the self-powered biosensor would be reduced. Different from the report of Zhang et al,[15] in this self-powered PEC sensing platform, the peroxidase-like catalytic activity of $Bi^{(+3-X)}$ is not strong than the O_2 consumption rate of GOD. Consequently, in the proposed PEC self-powered sensing system, the photocurrent decreassed with the increasing concentration of glucose could assign to the decomposition of glucose in the electrolyte consumed the dissolved oxygen (electron acceptors).

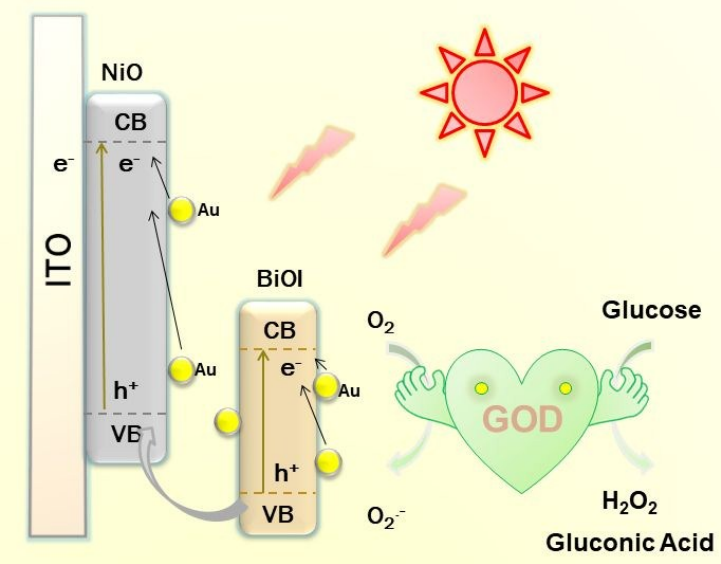

Scheme 2. Schematic illustration of the mechanism for the self-powered PEC sensing platform.

PEC characterization of fabricated biosensor

To further explore the sensitivity of the Au@BiOI/NiO photocathode toward dissolved oxygen, we did the contrast test (Figure 5A). GOD can consume oxygen in the process of glucose oxidation, generate H_2O_2 and gluconic acid at the same time. 1 mM H_2O_2 was added to the N_2 saturated buffer solution (blue curve), compared with the photocurrent of the N_2 saturated buffer solution (red curve), no obvious change was found. As depicted in Figure 5A, the air statured buffer solution (black curve) exhibited the highest photocurrent, which is bigger than N_2 statured buffer solution (red curve) and the containing 1mM H_2O_2 N_2 statured (blue curve) buffer solution. This result agreed with previous reports,[32] which demonstrated that in the proposed PEC sensing system the dissolved O_2 has greater effect than H_2O_2 on the cathodic

current. For comparison, the *I*−*V* curves of Au@BiOI/NiO/ITO hybrid electrode were measured with light (black curve) as well as without light (red curve), and the results are depicted in Figure 5B. Over the entire range (- 0.2 ~ 0.2 V), as the applied potential increased both curves increased as well. Under light illumination (black curve) the photocurrent density was bigger than that without light, indicating the PEC effect enhanced the generation of cathodic photocurrent. Apparently, light is an important factor to actuate the proposed self-powered PEC sensing platform.

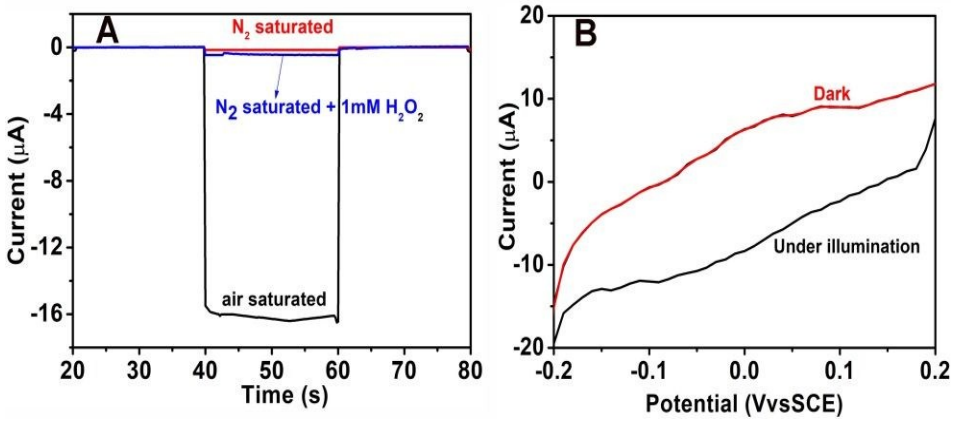

Figure 5. (A) The photocurrent performance of Au@BiOI/NiO in air saturated (black curve) and deaerated 0.1 M Tris-HCl solution (pH = 7.0) before (red curve) and after (blue curve) the injection of 1 mM H_2O_2. (with 0 V applied potential vs SCE and a LED light source. (B) The influence of light/without light on the *I-V* characteristic curves in the applied range (- 0.2 ~ 0.2 V).

For catching more detailed information about the matrix, the PEC performances of the each layer in the matrix were also investigated. As depicted in Figure 6A, under visible light irradiation, the NiO/ITO (curve a) showed a low current (~ - 150 nA), while after the modification of BiOI (curve b) a significant increase in photocurrent was observed. This could be attributed to the BiOI enhanced the light absorbance of NiO and sensitized the wide bandgap NiO. With the further modification of Au NPs, the photocurrent reached about - 16.4 μA. The reason might be the SPR effect of Au NPs as well as its good electron conductivity.[27] Curve d is the photocurrent response of GOD-Au@BiOI/NiO/ITO, which is lower than curve c (photocurrent response of Au@BiOI/NiO/ITO), indicating the successful modification of GOD (protein is non-conductive). Figure 6B is the corresponding EIS Nyquist plots of Figure 6A, as can see from the plot, the semicircle part (electron transfer resistance) of black curve (NiO/ITO) is smaller than the red curve (BiOI/NiO/ITO), which indicating the BiOI

was successfully modified. This is because the addition of semiconductor (BiOI) increased the electron transfer resistance (R_{et}). While after the addition of Au NPs (blue curve), the semicircle part is reduced, this could be attribute to the excellent conductivity of Au NPs. When the GOD was fixed on the surface of Au@BiOI/NiO/ITO (green curve), the semicircle part further enlarged, this could be attributed to the GOD (protein) blocked the transfer of electrons. Inset in Figure 6B is the equivalent circuit diagram of EIS, consist of solution resistance (R_s), R_{et}, Warburg impedance (Z_w) and the double layer capacitance (C_{dl}). Amongst them is R_{et}, the most important indicator for the electrodes interface properties. And the values of them were simulated by ZsimpWin (simulation software) and depicted in Table S1 (Supporting information). Figure 6C showed the output signal of the Au@BiOI/NiO/ITO electrode with repeated "on 20 s - off 20 s - on 20 s" light irradiation for 420 s. As can be seen, the signal curve of each independent cycle is homologous, which demonstrated the good signal output stability of the Au@BiOI/NiO/ITO electrode.

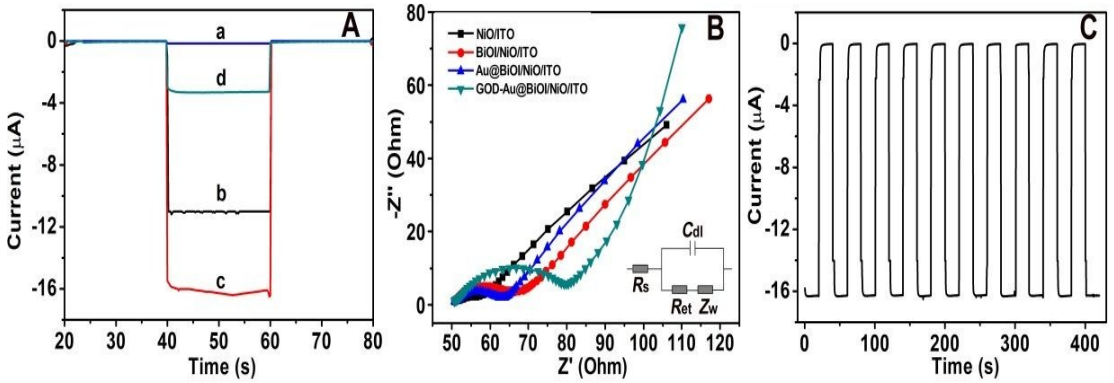

Figure 6. (A) Photocurrent performance of (a) NiO/ITO (b) BiOI/NiO/ITO (c) Au@BiOI/NiO/ITO (d) GOD-Au@BiOI/NiO/ITO; The applied voltage is 0 V.（B）and the corresponding EIS Nyquist plots (inset is the randles equivalent circuit of EIS). （C） PEC responses of the Au@BiOI/NiO/ITO electrode under several "on-off-on" irradiation cycles for 420 s (the applied voltage is 0 V).

Conditional selection for experiment

In order to acquire the optimum detectable signals, some external experimental conditions for the self-powered PEC platform need to be investigated. First, we studied the effect of the CBD cycles on the photocurrent response of the self-powered

sensing system. As depicted in Figure 7A, when the CBD cycles were 4, the BiOI/NiO in Tris-HCl exhibited the biggest photocurrent (~ - 10.5 μA). With the CBD cycles further increased, the photocurrent decreased, this could be attributed to the excess BiOI difference in size, shape and disordered distributing impeded the electron transfer rate. As shown in Figure S3, with the increase of CBD cycles the BiOI gradually grown on the surface of NiO. When the CBD cycles excess 4, the morphology of BiOI/NiO become disorganized. Thus, 4 cycles were used for the deposition of BiOI.

The dip-coating times of Au NPs was also optimized. As shown in Figure 7B, as the dipping times increased the photocurrent gradually enlarged and obtained a maximum photocurrent (~ - 16.4 μA) at 4 dip-coating times, and then reduced gradually. The reason might be that the excess Au NPs accelerated the e^-/h^+ recombination rate and reduced the photocurrent. For the best PEC performance, 4 times dipping was chosen for the decoration of Au NPs.

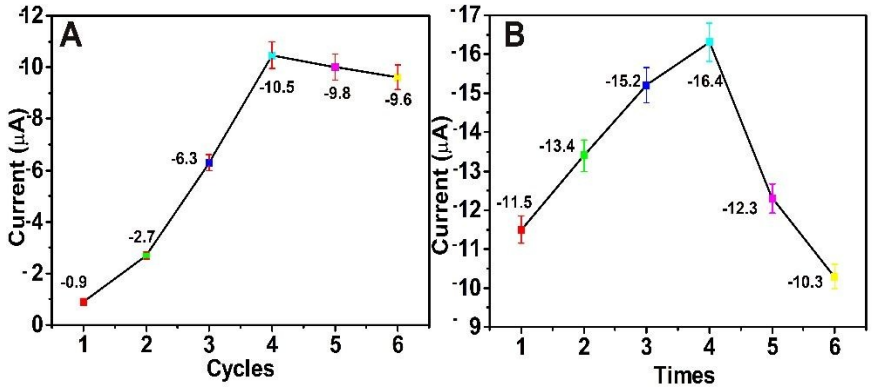

Figure 7. Effects of (A) the BiOI CBD repeating cycles, and (B) the Au NPs dip-coating times on the PEC performance of the self-powered platform. The applied voltage is 0 V.

Characterization of analytical performance

Under the optimized experiment conditions, we investigated the analytical performance of the self-powered PEC biosensor by detecting glucose with different concentrations. The photocurrent response of the biosensor changed regularly toward the concentration of glucose. Figure 8A depicted that the photocurrent decreased with the increasing concentration of glucose. As mentioned previously, with the concentration of glucose increased the competition between the photocathode and

View Article Online
DOI: 10.1039/C9NA00394K

GOD was also heating up. The higher the concentration of glucose is, the more dissolved O_2 (electron acceptors) would be consumed by GOD. As depicted in the diagram, the photocurrent response linearly decreased with the increasing logarithm of glucose in the range of $1 \times 10^{-7} \sim 5 \times 10^{-2}$ M. The calibration equation was ΔI = - 0.45 lg c - 3.7905, with the correlation coefficient of 0.992. Estimated according to the previous method of signal-to-noise ratio of 3:1 (S/N = 3),[13, 33] the limit of detection (LOD) was 8.71×10^{-8} M. Compared with many previously reports for the determination of glucose (Table S2), our work showed a wider dynamic linear range and lower LOD, indicating its advances in glucose analysis. Inset of Figure 8A is the corresponding photocurrent response. The selectivity of the proposed PEC biosensor was carried out, and the results were shown in Figure 8B. There were several coexisting interfering species, involving NaCl, dopamine and several amino acids were used for the test. Except for the interfering substances, all the tests were operated under identical experimental conditions. In this anti-interference experiment, the concentration of glucose and the interfering species both were 1 mM. Apparently except for the glucose (bar a) the other substances had no distinct influence, indicating the excellent selectivity of this self-powered PEC biosensor.

To evaluate the reproducibility of this self-powered sensing platform, we did the intra-assay and inter-assay test. The intra-assay was operated by testing five times with the concentrations of 3 mM and 6 mM glucose, from which the obtained relative standard deviation (RSDs) values were 4.7% and 4.3%, respectively. Under exactly the same conditions, five electrodes were used to measure one sample for the inter-assay, the resulting RSDs values were 4.9% and 5.1%, respectively. These results indicated the applicability potential of the proposed system for future utilization._In order to prove the feasibility of GOD-Au@BiOI/NiO electrode in the routine analysis, the proposed biosensor was used to detect the diluted glucose injections. As depicted in Table S3, the diluted glucose injections were measured by adding standard samples with different glucose levels for the recovery experiment. The obtained experimental results demonstrated that the proposed PEC biosensor has acceptable accuracy, which indicating its potential for biological applications.

View Article Online
DOI: 10.1039/C9NA00394K

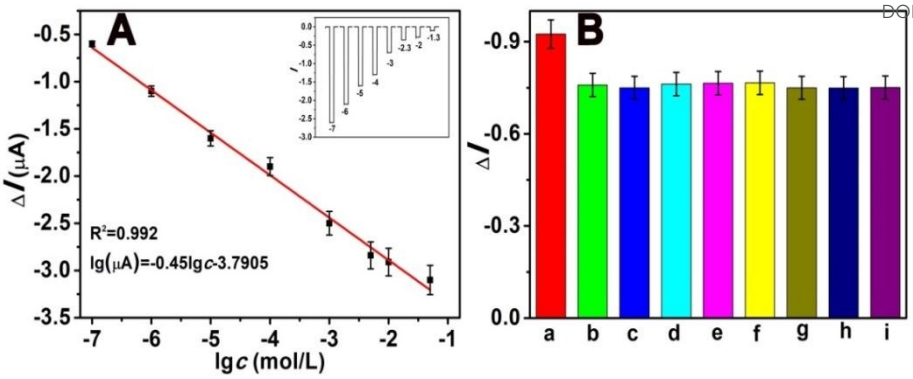

Figure 8. (A) The photocurrent decrease ($\Delta I = I_0 - I$) of the GOD modified Au@BiOI/NiO/ITO electrode vs - log $c_{glucose}$. I_0 and I are the photocurrents of the GOD-modified electrodes pre-and post-reaction with glucose, respectively. Inset is the corresponding photocurrent response for different concentrations of glucose; The applied voltage is 0 V. (B) Effect of added substances (1 mM): (a) glucose, (b) NaCl, (c) KCl, (d) ascorbic acid (AA), (e) dopamine, (f) urea, (g) L -valine, (h) L -lysine, (i) mixture (glucose + (b-h)), on the photocurrent response of the GOD-Au@BiOI/NiO/ITO electrode.

Conclusions

In summary, we developed a novel self-powered PEC biosensing platform based on 0D Au@ 3D BiOI/2D NiO/ITO photocathode, and demonstrated the construction and characterization of the hybrid nanocomposite. The obtained experimental results indicated the ideal coupling between 0D Au NPs QDs, 3D BiOI NFs and 2D NiO NSAs. Owing to the sensitization effect of BiOI as well as the SPR effect and good conductivity of Au NPs, the constructed 0D Au@3D BiOI/2D NiO/ITO photocathode showed excellent PEC activities and oxygen sensitivity. The self-powered PEC sensing platform also exhibited high sensitivity and good anti-interference when it was used to detect glucose in vitro. Besides, the fabricated PEC biosensor was also successfully used for the detection of glucose injections, the results indicated that the proposed Au@BiOI/NiO photocathode have a promising prospect in the self-powered PEC biosensing devices. More generally, this work proved that the heterostructures and materials combination design are still an efficient method for improving the performance of PEC biosensing devices.

Conflicts of interest

The authors declare no competing financial interest.

View Article Online
DOI: 10.1039/C9NA00394K

Acknowledgment

We are very grateful to National Natural Science Foundation of China (Grant no. 21775054), the Natural Science Foundation of Shandong Province (Grant no. ZR2016JL013).

Notes and references

1. R. L. Arechederra and S. D. Minteer, *Anal. Bioanal.Chem.*, 2011, **400**, 1605-1611.
2. M. Grattieri and S. D. Minteer, *ACS Sens.*, 2018, **3**, 44-53.
3. K. Zhao, X. Yan, Y. Gu, Z. Kang, Z. Bai, S. Cao, Y. Liu, X. Zhang and Y. Zhang, *Small*, 2016, **12**, 245-251.
4. Z. Kang, Y. Gu, X. Yan, Z. Bai, Y. Liu, S. Liu, X. Zhang, Z. Zhang, X. Zhang and Y. Zhang, *Biosens. Bioelectron.*, 2015, **64**, 499-504.
5. B. Çakıroğlu and M. Özacar, *Biosen. Bioelectron.*, 2018, **119**, 34-41.
6. W. W. Zhao, J. J. Xu and H. Y. Chen, *Chem. Soc. Rev.*, 2015, **44**, 729-741.
7. C. Li, C. Han, Y. Zhang, Z. Zang, M. Wang, X. Tang and J. Du, *Sol. Energy Mater. Sol. Cells*, 2017, **172**, 341-346.
8. A. Devadoss, P. Sudhagar, C. Terashima, K. Nakata and A. Fujishima, *J. Photochem. Photobiol. C*, 2015, **24**, 43-63.
9. B. Peng, L. Tang, G. Zeng, S. Fang, X. Ouyang, B. Long, Y. Zhou, Y. Deng, Y. Liu and J. Wang, *Biosens. Bioelectron.* 2018, **121**, 19-26.
10. I. C. Wu, Y. H. Weng, M. Y. Lu, C. P. Jen, V. E. Fedorov, W. C. Chen, M. T. Wu, C. T. Kuo and H. C. Wang, *Opt. Express*, 2017, **25**, 7689-7706.
11. K. Yan, Y. Yang, Y. Zhu and J. Zhang, *Anal. Chem.,* 2017, **89**, 8599-8603.
12. W. X. Dai, L. Zhang, W. W. Zhao, X. D. Yu, J. J. Xu and H. Y. Chen, *Anal. Chem.* 2017, **89**, 8070-8078.
13. Q. Han, R. Wang, B. Xing, H. Chi, D. Wu and Q. Wei, *Biosens. Bioelectron.,* 2018, **106**, 7-13.
14. Q. Han, R. Wang, B. Xing, T. Zhang, M. S. Khan, D. Wu and Q. Wei, *Biosens. Bioelectron.*, 2018, **99**, 493-499.
15. L. Zhang, Y. F. Ruan, Y. Y. Liang, W. W. Zhao, X. D. Yu, J. J. Xu and H. Y. Chen, *ACS Appl. Mater. Interfaces*, 2018, **10**, 3372-3379.
16. K. Kim, H. Kim, H. Jang, J. Park, G.-Y. Jung and M. G. Kim, *ACS Appl. Mater. Interfaces*, 2018, **10**, 39487-39493.
17. Z. Kang, X. Yan, Y. Wang, Y. Zhao, Z. Bai, Y. Liu, K. Zhao, S. Cao and Y. Zhang, *Nano Res.*, 2016, **9**, 344-352.
18. G. K. C. dos Santos, F. G. S. da Silva, S. Yotsumoto Neto, W. T. P. dos Santos, R. de Cássia Silva Luz and F. S. Damos, *Electroanalysis*, 2018, **30**, 1750-1756.
19. R. Li, Y. Zhang, W. Tu and Z. Dai, *ACS Appl. Mater. Interfaces*, 2017, **9**, 22289-22297.
20. K. Yan, Y. Yang, O. K. Okoth, L. Cheng and J. Zhang, *Anal. Chem.*, 2016, **88**,

View Article Online
DOI: 10.1039/C9NA00394K

6140-6144.

21. M. G. Kibria, F. A. Chowdhury, S. Zhao, B. AlOtaibi, M. L. Trudeau, H. Guo and Z. Mi, *Nat. Comm.*, 2015, **6**, 6797.
22. L. Yosefi and M. Haghighi, *Appl. Catal. B.*, 2018, **220**, 367-378.
23. G. C. Fan, X. M. Shi, J. R. Zhang and J. J. Zhu, *Anal. Chem.*, 2016, **88**, 10352-10356.
24. Y. Ku, C. N. Lin and W. M. Hou, *J. Mol. Catal. A Chem.*, 2011, **349**, 20-27.
25. Y. Zhang, Q. Pei, J. Liang, T. Feng, X. Zhou, H. Mao, W. Zhang, Y. Hisaeda and X. M. Song, *Langmuir*, 2015, **31**, 10279-10284.
26. Y. Dou, J. Zhou, A. Zhou, J. R. Li and Z. Nie, *J. Mater. Chem. A*, 2017, **5**, 19491-19498.
27. S. Eustis and M. A. El Sayed, *Chem. Soc. Rev.*, 2006, **35**, 209-217.
28. J. Wu, C. Luo, D. Li, Q. Fu and C. Pan, *J. Mater. Sci.*, 2017, **52**, 1285-1295.
29. K. H. Ye, Z. Chai, J. Gu, X. Yu, C. Zhao, Y. Zhang and W. Mai, *Nano Energy*, 2015, **18**, 222-231.
30. W. Wang, Y. Liu, C. Xu, C. Zheng and G. Wang, *Chem. Phys. Lett.,* 2002, **362**, 119-122.
31. R. E. Dietz, G. I. Parisot and A. E. Meixner, *Phys. Rev. B*, 1971, **4**, 2302-2310.
32. W. W. Zhao, J. Wang, Y. C. Zhu, J. J. Xu and H. Y. Chen, *Anal. Chem.*, 2015, **87**, 9520-9531.
33. Y. Liu, K. Yan and J. Zhang, *ACS Appl. Mater. Interfaces*, 2016, **8**, 28255-28264.

View Article Online
DOI: 10.1039/C9NA00394K

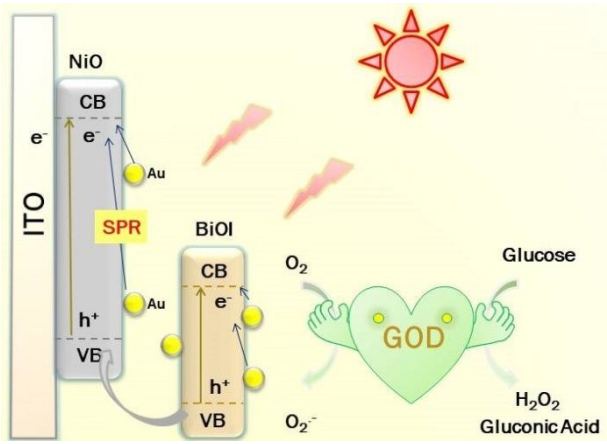

SPR enhanced self-powered PEC sensing platform for glucose detection